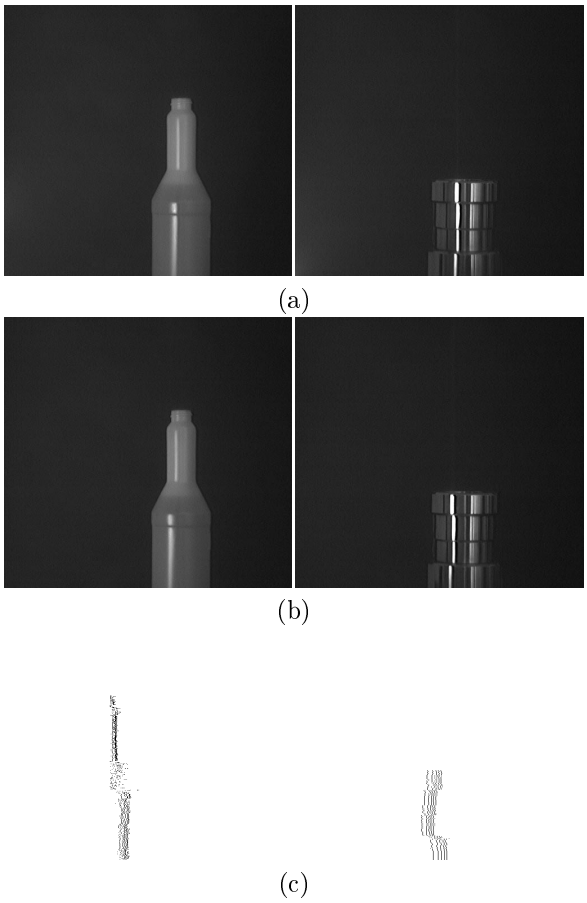

Figure 8: Examples of a plastic bottle and a metallic cylinder: (a) Images with illumination along S1. (b) Images taken with illumination 15 degrees away from S1. (c) Recovered depths for some contours

3.4 Experimental Results

We use a plastic bottle and a metallic cylinder as examples to show shape reconstruction using active illumination (See Figure 8). The illumination light source is approximated as a long vertical light source. Consecutive images were captured with the illumination angle changed in increments of 5 degrees on a horizontal plane. The angle θ_0 in Figure 6 is 10 degrees. The coordinates, or 3D depth of the initial point P_0 is recovered with the shape from occluding contours and highlights method described in the previous section in Figure 1, where ϕ is 80 degrees.

The ratios found from the reconstructed plastic bottle are 1:1.73:3.74 compared with the real ratios 1:1.16:2:29. The ratios from the reconstructed metallic cylinder are found as 1:0.86:0.81:1.14 compared with the real ratios 1:0.88:0.86:1.08. As in the first method, the results are noisy in the transitional regions due to the use of a vertical light source. These errors can be avoided by using a point illumination source and applying the proposed 3D surface recovery method.

4 Discussion and Conclusion

In this paper, we explored two simple mathematical solutions for 3D shape reconstruction from highlights and occluding contours using active camera and illumination control. When the results from the proposed methods are compared, it is seen that the second method using illumination control is noisier. The explanation for this is two-fold: first, saturation of highlights results in imprecise localization; second, the initial point in the second method is computed using results from the first method and thus errors from the previous step propagate into the results.

Experimental results support the presented mathematical derivations. A relation between the minimum illumination angle change and the detectable surface normal curvature, was also presented. This result can be used to control the illumination angle under different surface structures.

References

[1] E. Hecht. *Optics*. Addison-Wesley Publishing, 1990.

[2] J. J. Koenderink. What does the occluding contour tell us about solid shape? *Perception*, 13, 1984.

[3] K. N. Kutulakos. Exploring three-dimensional objects by controlling the point of observation. *PhD thesis, University of Wisconsin-Madison*, 1994.

[4] J. Maver and R. Bajcsy. Occlusions as a guide for planning next view. *IEEE Trans. on Pattern Analysis and Machine Intelligence*, 15(5):417–433, 1993.

[5] M. Oren and S. K. Nayar. A theory of specular surface geometry. *Proc. ICCV*, pages 740–743, 1995.

[6] G. Turk and M. Levoy. Zippered polygon meshes from range images. *Proc. SIGGRAPH'94*, pages 311–318, 1994.

[7] P. Whaite and F. P. Ferrie. From uncertainty to visual exploration. *IEEE Trans. on Pattern Analysis and Machine Intelligence*, 13(10):1038–1049, 1991.

[8] X. Yi and O. Camps. Robust occluding contour detection using the Hausdorff distance. In *IEEE Conference on Computer Vision and Pattern Recogntion*, pages 962–968, June 1997.

[9] J. Y. Zheng, Y. Fukagawa, and N. Abe. Shape and model from specular motion. *Proc. ICCV*, pages 72–79, 1995.

[10] J. Y. Zheng, Y. Fukagawa, T. Ohtsuka, and N. Abe. Acquiring 3d models from rotation and highlights. *Proc. International Conference on Pattern Recognition*, pages 331–336, 1994.

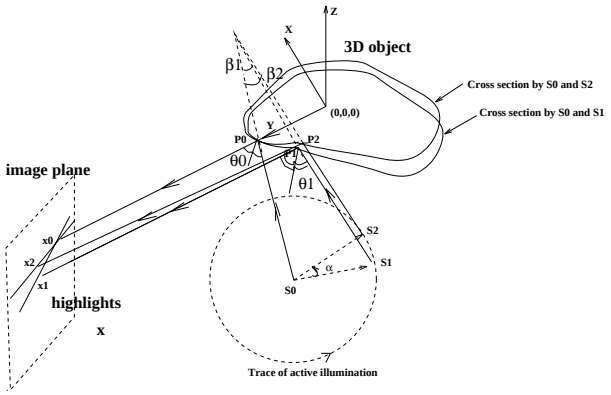

Figure 6: 3D shape from active illumination.

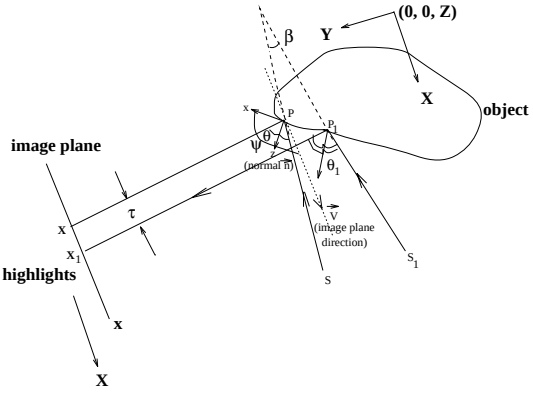

Figure 7: Relation between surface curvature and illumination.

plane of S_0 and S_2. The new cross section becomes a new 2D curve. The depths of the local points around P_0 along this 2D curve can be computed as described in the previous section. Thus, the depths of the points on the surface around P_0 can be computed by changing the angle α up to 180 degrees.

3.3 Minimum illumination change

The *observable* movement of the specular highlight on the images is related to the surface curvature and the illumination angle change. If the illumination angle change is too small, we may not observe the position change of the specular highlights on the image. Also, the illumination angle change should be larger for larger surface normal curvatures in order to obtain the same amount of specular highlight shift as that in the case of smaller surface normal curvatures.

In the following, we develop a mathematical relation among the surface normal curvature, illumination angle change, and the specular highlight shift. Consider a 2D plane where the light source moves on as shown in Figure 7. The images of the specular highlight will also shift on that plane. In the 3D case, as discussed in the previous section, we actually deal with slices of 2D planes. This is similar to the assumption of epipolar plane when we move the camera around for 3D reconstruction.

When the illumination angle is along S, the highlight is at point P and it is observed on the image plane at location X. When the illumination angle is changed by β to S_1 angle, the highlight moves to point P_1 and it is observed at location X_1 on the image plane. As shown in the Figure 7, let P be the origin of the Cartesian coordinate system xz where z is along the normal direction, the $x-z$ plane is along the normal plane and $x-y$ is the tangent plane at P. The normal plane meets the object on the normal curve with normal curvature K_t. By neglecting the third-order and higher order terms, Koenderink[2] showed that the tangents of the normal curve at P can be described as:

$$\frac{\partial z}{\partial x} = K_t x \tag{15}$$

Let τ be the distance between X and X_1, $\tau = |X - X_1|$. Then, we need to find out the relationship between τ, β, and K_t.

From Figure 7 it is seen that, in xz coordinates, the image plane (actually it is a 1D line in this case) is in the direction $\vec{V}$ forming an angle of $\pi/2$ plus θ plus the angle between $\vec{V}$ and $\vec{S}$ with respect to $+x$ direction. Thus, the total angle ψ is $\pi - \theta$ for $\vec{V} = (-\cos\theta, \sin\theta)$. As it was seen before, the angle between the normals at P_1 and P is equal to $\beta/2$. Therefore, the normal at P_1 has an angle of $\pi/2 + \beta/2$ with respect to $+x$ direction. The tangent line at P_1 has slope $-1/\tan(\pi/2 + \beta/2)$, or $\tan\beta/2$. Equating this value with Equation (15), the coordinates of P_1 are $\vec{P_1} = (\frac{\tan(\beta/2)}{K_t}, \frac{\tan^2(\beta/2)}{2K_t})$.

Finally, τ, or the projection of $\vec{P_1}$ onto $\vec{V}$ is given by

$$\tau = \vec{P_1} \cdot \vec{V} = \frac{\tan(\beta/2)}{K_t}(-\sin\theta + \frac{\sin\theta\tan(\beta/2)}{2}) \tag{16}$$

In the case of orthographic projection, this is the observed movement of the highlight on the image. In the case of perspective projection[1], the observed change is modified by a factor of $\frac{f}{u-f}$, where f is the focal length, u is the objective distance for P and P_1 with the assumption that P and P_1 are very close to each other.

Equation (16) shows that, with the same illumination angle change, smaller surface normal curvature will result in larger specular highlight shift; and that with the same normal curvature, a larger illumination angle change will result in a larger specular highlight shift.

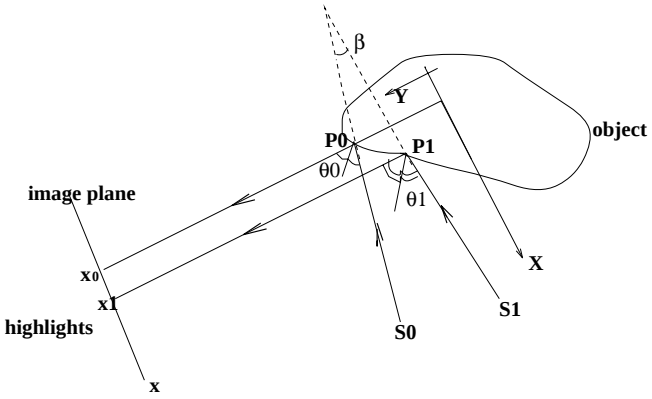

Figure 5: Using two different illumination directions.

P_0 has surface normal direction on the XY plane. P_0 is the highlight point when the illumination is located at S_0. Point P_1 is a point very close to P_0, and it is the highlight point when the illumination moves to the S_1 direction. Therefore, if the normal angle at P_0 is θ_0, and at P_1 is θ_1, $\theta_1 = \theta_0 + \beta/2.0$.

If the coordinate system is such that point $P_0 = [X_0 Y_0]^t$, we have from Equation (8):

$$\begin{bmatrix} \rho_0 \\ \rho_0' \end{bmatrix} = \begin{bmatrix} \cos\theta_0 & \sin\theta_0 \\ -\sin\theta_0 & \cos\theta_0 \end{bmatrix} \begin{bmatrix} X_0 \\ Y_0 \end{bmatrix} \tag{10}$$

Assuming point $P_1 = [X_1 Y_1]^t$, we have:

$$\begin{bmatrix} X_1 \\ Y_1 \end{bmatrix} = \begin{bmatrix} \cos\theta_1 & -\sin\theta_1 \\ \sin\theta_1 & \cos\theta_1 \end{bmatrix} \begin{bmatrix} \rho_1 \\ \rho_1' \end{bmatrix} \tag{11}$$

From the images taken for the two illumination directions, we can measure the displacement x in the camera coordinate system for the highlights corresponding to P_0 and P_1. In the case of orthographic projection, $X_1 = x$. Therefore, X_1 is a known constant in Equation (11). Equation (11) is a first order differential equation for ρ_1. By solving it, we have,

$$\rho_1 = C_1 \sin\theta_1 + X_1 \cos\theta_1 \tag{12}$$

where C_1 is a constant depending on the initial condition. However, if β is very small, we can approximately take, $\rho_{1|_{\theta 1 = \theta 0}} = \rho_0$ and

$$C_1 = Y_0 + (X_0 - X_1)\cos\theta_0 / \sin\theta_0$$

At this point, ρ_1 is solved completely. Using equations 8 and 12, we solve the Y coordinate at point P_1 as $Y_1 = Y_0 + (X_0 - X_1)\cos\theta_0/\sin\theta_0$. The general solution for the coordinates of any point $P_n = (X_n, Y_n)$ can be solved in a similar way where the constant term in Equation (12) is solved using the assumption: $\rho_{n|_{\theta n = \theta n-1}} = \rho_{n-1}$ Thus, the final solution is obtained as:

$$P_n = \begin{bmatrix} X_n \\ Y_{n-1} + (X_{n-1} - X_n)\cos\theta_{n-1}/\sin\theta_{n-1} \end{bmatrix} \tag{13}$$

where X_n is measured from the images and $\theta_n = \theta_{n-1} + \beta/2.0$. Therefore, as long as the coordinates and surface normal for the initial point P_0 are known, the coordinates of all the boundary points close to P_0 can be recovered by repeatedly using Equation (13).

Next, we analyze the robustness of the proposed method. For the point P_n, the error of its X_n coordinate comes from errors in the measurement of the highlight locations on the captured image. The error of its Y_n coordinate, however, comes from Y_{n-1}, X_n, X_{n-1}, and θ_{n-1}. Thus, this error is the result of accumulations of the errors of the previous recovered points, due to the errors in the measurement of the highlight locations and the illumination angles.

Suppose that at each new illumination direction S_n we measure its illumination angle by adding the angle of the previous illumination angle θ_{n-1} and the illumination angle change β. From Equation (13), the error of measured illumination angle change θ propagates accumulatively to each of the new boundary points P_n. This can also be seen by taking the partial derivative of Y_n with respect to β.

$$\frac{\partial Y_n}{\partial \beta} = \frac{\partial Y_{n-1}}{\partial \beta} - (X_{n-1} - X_n)\frac{1}{\sin^2\theta_{n-1}}\frac{\partial \theta_{n-1}}{\partial \beta} \tag{14}$$

If we keep expanding this equation, we will add more errors due to the error propagation from the previous points. This can be very severe for the boundary points recovered later. However, if at each new illumination direction S_n, we measure its angle θ_n with respect to the initial illumination direction S_0 instead of measuring it from the previous direction S_{n-1}, we can greatly reduce the accumulative error. In this case, the computed error of Y_n will come from θ_{n-1} only, and θ_{n-1} is measured once instead of accumulatively added by β.

3.2 3D surfaces

For the 3D case, the local depth can be computed by simply rotating a point light source around the original illumination direction, and deviating the rotation angle from the original angle by β. This is shown in Figure 6, where S_0 is the original illumination, S_2 is the new illumination direction, and α is the rotation angle.

At the new illumination S_2, we can find a new cross section or normal plane of the 3D object through the

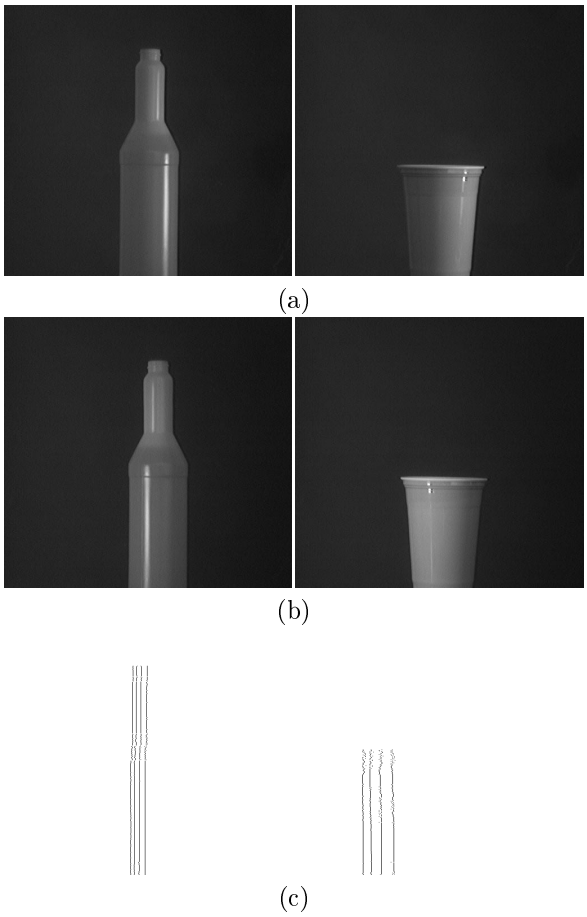

Figure 3: Examples of a plastic bottle and a plastic cup: (a) Images taken when the camera is at the location A. (b) Images taken when the camera is at the location B. (c) Recovered depths for some contours

mals are not along horizontal plane. Therefore, the detected intensity peaks from the captured images do not really correspond to the defined highlight locations but a noisy peak. To be more precise, we can not really find a pulse shape distribution of the intensity values on the image when there is actually no specular highlights happening. For a complicated shape object, a point illumination source is a better choice, since we can move it on the slices of 3D space, and recover the corresponding 2D curves of the object along each slice.

3 Using Active Illumination

In this section we will explore an alternative method for obtaining local curvature at specular highlight areas on the surface by using active illumination control.

In this method, the camera is fixed at one location when the reconstruction process for one aspect of the object is performed. However, the illumination is moved around the object in a controlled way. A sequence of images is taken as the illumination direction is changed. The illumination is assumed to come from far away such that its rays are along one direction, and the projection is assumed to be orthographic. The maximum reflection (specular highlight) happens when the incidence angle is equal to the reflection angle. We first consider the case of a $2D$ object or $2D$ curve/boundary, and then extend it to the general $3D$ case.

3.1 2D curves

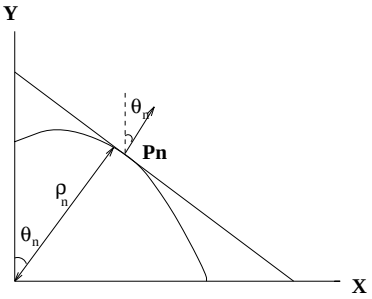

Figure 4: Representation of a point using ρ_n and θ_n.

A curve can be represented in a way, similar to the Legendre transformation, as illustrated in Figure 4 [5]. Let $P_n = (X_n, Y_n)$ be a point on the curve, and ρ_n be the distance from the origin to the tangential line at P_n. Let θ_n be the angle between the normal at P_n, n, and the tangential line. Then, the function $\rho_n(\theta_n)$ and its derivative $\rho'_n(\theta_n)$ with respect to θ_n are expressed in terms of X_n and Y_n by:

$$\begin{bmatrix} \rho_n \\ \rho'_n \end{bmatrix} = \begin{bmatrix} \cos\theta_n & \sin\theta_n \\ -\sin\theta_n & \cos\theta_n \end{bmatrix} \begin{bmatrix} X_n \\ Y_n \end{bmatrix} \quad (8)$$

The inverse transformation is obtained as:

$$\begin{bmatrix} X_n \\ Y_n \end{bmatrix} = \begin{bmatrix} \cos\theta_n & -\sin\theta_n \\ \sin\theta_n & \cos\theta_n \end{bmatrix} \begin{bmatrix} \rho_n \\ \rho'_n \end{bmatrix} \quad (9)$$

We first define an object centered coordinate system as $X - Y - Z$ and a camera centered (image plane) coordinate system as $x - y$. Suppose we have an infinite long light source along the Z axis that can rotate along the $+Z$ direction, and that the camera viewing direction is along the $-Y$ direction. The normal plane or cross section over $X - Y$ plane of this configuration is shown in Figure 5. We also assume that the angle between illumination S_0 and S_1 is β, and that point

As a result, we can find the coordinates of the object points on the surface.

Equation (3) gives a simple closed form solution for the recovery of X and Y. The coordinates X and Y are linearly related with the measured x_1 and x_2. X and Y are also a function of ϕ – the angle between the illumination direction and the camera viewing direction. Thus, the error of the angle ϕ directly effects the outcome of the computed result. Next, we derive the relation between the error of the computed depth and the error of the measured ϕ.

Taking the partial derivative of Equation (3) with respect to the error of ϕ, we have:

$$\frac{\partial X}{\partial \phi} = \frac{(x_1 + x_2 \cos\phi)\sin\theta}{\sin^2\phi} \tag{4}$$

$$\frac{\partial Y}{\partial \phi} = -\frac{(x_1 + x_2 \cos\phi)\cos\theta}{\sin^2\phi} \tag{5}$$

From Equations (4) and (5), we obtain a simple sine and cosine relationship for the absolute errors of X and Y, respectively. An interesting case is when θ is 0; in this case there is no direct effect between the error of X and the error of ϕ since $\frac{\partial X}{\partial \phi}$ is zero. However, the outcome effect of the error of Y from ϕ is maximized. A similar case is when θ is $\pi/2$, and the recovered Y value is not affected.

Using Equations (3), (4), and (5), we obtain the expression for the relative depth values of X and Y:

$$\frac{\frac{\partial X}{\partial \phi}}{X} = \frac{(\frac{x_1}{x_2} + \cos\phi)\sin\theta}{(\frac{x_1}{x_2}\sin(\phi-\theta) - \sin\theta)\sin\phi} \tag{6}$$

$$\frac{\frac{\partial Y}{\partial \phi}}{Y} = \frac{(\frac{x_1}{x_2} + \cos\phi)\cos\theta}{(\frac{x_1}{x_2}\cos(\phi-\theta) + \cos\theta)\sin\phi} \tag{7}$$

These two expressions give the relative errors for the coordinates of X and Y when the camera viewing angle has an error of one degree. Figure 2 shows plots of these two errors with respect to the viewing angle ϕ under different $\frac{x_1}{x_2}$ ratios, with the angle of θ chosen as 45 degrees.

From Figure 2, the following observations can be made on the relative errors of X and Y: (1) The relative error of X changes differently for different values of the viewing angle ϕ. When this angle is less than approximately 50 degrees, the errors are large, and disordered. However, the error becomes very small when ϕ is between 50 and 80 degrees. (2) The relative error of Y changes in a different fashion with respect to ϕ. For different ratios of $\frac{x_1}{x_2}$, it decreases very slowly with respect to ϕ. Also the values of $\frac{x_1}{x_2}$ do not have a big impact on this relationship. (3) The relative errors for both X and Y are close to zero when ϕ is between 50 and 80 degrees. Therefore, it is always a better choice to control the angle between the viewing direction and illumination direction within this range. This can be done by actively adjusting the illumination direction to a new direction when ϕ is off this range.

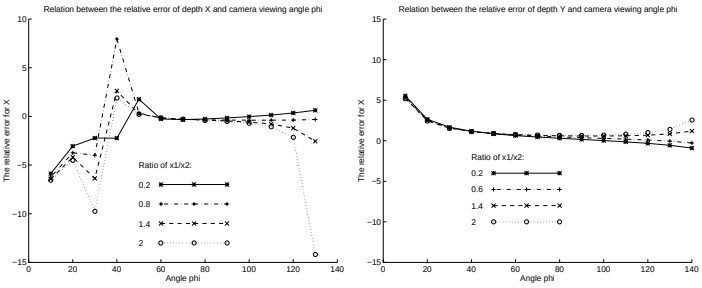

(a) (b)

Figure 2: The relative errors of X and Y w.r.t. ϕ.

2.3 Experimental results

Two examples of this approach can be seen in Figure 3 for a plastic bottle and a plastic water cup. In these experiments, we use a vertical long light source and the camera is moved in increments of 5 degrees on a horizontal plane to capture sequences of images. The angle between the illumination and the camera viewing angle at location A is 70 degrees. The occluding contours were detected using a correlational method based on the Hausdorff distance [8].

Figures 3 (a) and (b)show the images when the camera is located at the locations A and B, respectively, as described in Figure 1. We processed 8 images with 4 consecutive images each at location A and B's neighborhood.

Since this approach is valid under orthographic projection, it is not possible to compare the real 3D depth values with the recovered ones. However, we can compare the correctness of the scaled dimensions. To do that, we can compute the ratios for the three cylinders forming the plastic bottle obtained using the reconstruction process with the ratios measured from the object. Using the least square method, we found out the ratios from the reconstructed data are 1:1.80:3.81. The ratios from the real plastic bottle are found as 1:1.75:3.65.

From the reconstructed images, it is seen that the cylindrical parts of the objects are recovered well. However, at the curved transitional parts, the reconstructed results are noisy. This is because we use a long vertical illumination light source whose illumination directions are well designed along the horizontal plane, but at the curved locations, the surface nor-

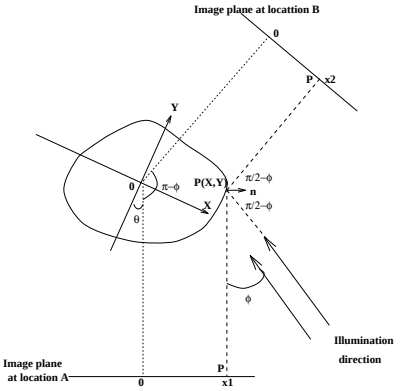

Figure 1: Highlight and occluding contour geometry.

proach has two problems. First, it is computational expensive, since it involves several integration and differentiation computations. Second, in order to mathematically express the solution uniquely, it has to solve a boundary condition, or to calculate the constant term for the image trajectory function. Oren solves this problem by tracking at least two virtual features which is also computational expensive. Zheng, on the other hand, fixes the camera and illumination and simply rotates the object. Even though Zheng's mathematical tool is simpler, it requires the use of two or more illumination sources to uniquely determine the solution.

Next, we present an approach that solve these problems by allowing the observer or camera to actively move around the object and using the occluding contour as a boundary condition or extra constraint to recover the 3D surface shape globally.

2.1 Highlights & Occluding Contours

Occluding contours provide surface normal information at the visible rim, while specular highlights occur when the illumination incidence angle equals the reflectance angle. Although there exists a strong relationship between occluding contours and highlights, they have not been used together for 3D reconstruction until now. Next, we explore this relationship and use it to develop a new 3D shape reconstruction algorithm.

We first explore how to use active sensor and illumination control to detect highlights based on known occluding contours. The main idea is to predict when an occluding contour in one image of a sequence of images will become a highlight in another image of the sequence.

We illustrate this idea by using Figure 1 for the 2D case where the 2D curve has a $X-Y$ coordinate system and the sliced image or normal plane image has a x coordinate system. In the sequel, we assume orthographic projection.

Suppose at location A, the camera viewing direction forms an angle of θ with the $+Y$ direction, and the illumination direction forms an angle of ϕ with the viewing direction. The direction of the sliced image, in the object centered coordinate system, is along $\hat{\mathbf{x_A}} = (\cos\theta, \sin\theta)$.

If at camera location A, a point $P(X,Y)$ is detected as a point on the visible rim, the surface normal at $P(X,Y)$ is known. The normal direction at $P(X,Y)$ forms an angle of $\pi/2-\phi$ with the illumination direction. In other words, the incidence angle for the illumination at point $P(X,Y)$ is $\pi/2-\phi$. Therefore, the specular component is reflected forming an angle of $\pi/2-\phi$ with the normal direction at $P(X,Y)$. It can be seen that, if the camera is moved to location B by moving around the object on the normal plane defined by the surface normal and the illumination direction to location B by an amount of $\phi+\pi/2-\phi+\pi/2-\phi = \pi-\phi$, the projection (image) of the point $P(X,Y)$ will become a highlight point. At camera location B, the direction of the sliced image, in the object centered coordinate system, is along $\hat{\mathbf{x_B}} = (\cos(\theta+\pi-\phi), \sin(\theta+\pi-\phi))$.

This shows that by tracking the occluding contours and moving the camera around the object, we can predict where the highlights will occur. Furthermore, the idea described above can be reversed, i.e. we can predict when a highlight in one image will become an occluding contour in another one.

2.2 Computing depth using both

The above relationship between occluding contours and highlights can be used to compute depth for the object surface points.

Consider two images of an object, one from location A and the other from location B. Let $x_A = (\cos\theta, \sin\theta)$ and $x_B = (\cos(\theta-\phi+\pi), \sin(\theta-\phi+\pi))$ be the directions of the sliced images at locations A and B, respectively. Let x_1 and x_2 be the image coordinates of an object point P with object coordinates (X,Y), respectively. Then,

$$x_1 = \mathbf{P}\cdot\mathbf{x_A} = X\cos\theta + Y\sin\theta \quad (1)$$
$$x_2 = \mathbf{P}\cdot\mathbf{x_B} = X\cos(\theta+\pi-\phi) + Y\sin(\theta+\pi-\phi)$$

If $\pi \neq \phi$, we can solve for X and Y,

$$X = \frac{1}{\sin\phi}(\sin(\phi-\theta)x_1 - \sin\theta x_2) \quad (2)$$
$$Y = \frac{1}{\sin\phi}(-\cos(\phi-\theta)x_1 + \cos\theta x_2) \quad (3)$$

3D Object Depth Recovery From Highlights Using Active Sensor And Illumination Control *

Xilin Yi[1] and Octavia I. Camps[1,2]
[1]Department of Electrical Engineering
[2]Department of Computer Science and Engineering
The Pennsylvania State University
University Park, PA, 16802
E-mails: {xilin,camps}@whale.ece.psu.edu

Abstract

Two approaches for 3D curved object reconstruction using *active sensor and illumination control* are proposed and compared to each other. In both cases, the highlight information is fully utilized rather than discarded, and knowledge of the object surface is not required. The first approach requires camera control only and recovers shape (depth) from highlights and occluding contours. The second approach requires both camera and illumination control and recovers 3D depth from highlights only. **KEY WORDS:** Shape reconstruction, specular reflection, highlights, active vision.

1 Introduction

Computer-aided designed (CAD) models are used in very diverse domains such as design and manufacturing, industrial inspection, autonomous navigation, vision systems, architecture, geographical information systems, and visual reality, just to mention a few. A method for automating the acquisition process of models is clearly desirable, especially for objects with complex surface geometry for which manual construction can be time-consuming.

Several studies have been reported [4, 7, 3] for automating model acquisition of complicated objects (e.g., with dents and holes), and commercial products for building models from real objects have appeared [6]. There are many factors that make the reconstruction task difficult. In particular, specular reflections which are present on most objects made of plastic and metal, can be misidentified as markings and occluding contours and cause problems while searching for correspondences between pair of images. Thus, traditionally specular reflections have been avoided by either treating the object surface, using polarized light or by some image pre-processing. However, specular reflections are usually the strongest features in an image, making them easy to detect, and they can provide rich qualitative (surface normal) and quantitative (depth and curvature) information about the local and global shape of the object.

In this paper, we propose and compare two approaches for 3D curved object reconstruction using *active sensor and illumination control*. In both cases, the highlight information is fully utilized rather than discarded. The proposed methods do not require to know the object surface properties and exploit relations between specular reflection and the camera view angle to reconstruct curved object surfaces at highlight locations. The first approach requires camera control only and recovers shape (depth) from highlights and occluding contours, where the occluding contours are identified by the method presented in [8]. The second approach requires both camera and illumination control and recovers 3D depth from highlights only. This method tracks the movement of specular highlights, and recovers the 3D depth from the amount of highlight shift.

2 Using Active Sensor

Quantitative 2D and 3D curve recovery from specular highlight has been studied by Oren [5] and Zheng [9, 10]. Oren uses support functions of curves to derive a close-form relation between the image trajectory of a virtual feature and the geometry of the specular surface it travels on. In this approach, the observer or camera moves actively around the object. This ap-

*This work was supported in part by NSF grant IRI9309100 and in part by Penn State University and HRB Systems through the Center for Intelligent Information Processing.